RESEARCH ARTICLE

Assessing the performance of a multi-nested ocean circulation model using satellite remote sensing and in situ observations

Shiliang Shan*, Jinyu Sheng, Kyoko Ohashi and Mathieu Dever

Department of Oceanography, Dalhousie University, Halifax, Nova Scotia, Canada, B3H 4R2

Abstract: This study presents a multi-nested ocean circulation model developed recently for the central Scotian Shelf. The model consists of four submodels downscaling from the eastern Canadian Shelf to the central Scotian Shelf. The model is driven by tides, river discharges, and atmospheric forcing. The model results are validated against observations, including satellite remote sensing data from GHRSST and Aquarius and in situ measurements taken by tide gauges, a marine buoy, ADCPs and CTDs. The ocean circulation model is able to capture variations of sea level, hydrography and the Nova Scotia Current on timescales of days to seasons over the central Scotian Shelf. Model results are used in a process study to examine the effect of tidal mixing and wind-driven coastal upwelling in the formation of cold surface waters along the coast of Nova Scotia.

Keywords: Scotian Shelf, nested-grid model, model validation, remote sensing, Nova Scotia Current

*Correspondence to: Shiliang Shan, Department of Oceanography, Dalhousie University, Halifax, Nova Scotia, Canada B3H 4R2; Email: sshan@dal.ca

Received: February 23, 2016; **Accepted:** April 15, 2016; **Published Online:** June 19, 2016

Citation: Shiliang Shan, Jinyu Sheng, Kyoko Ohashi *et al.*, (2016). Assessing the performance of a multi-nested ocean circulation model using satellite remote sensing and in situ observations. *Satellite Oceanography and Meteorology*, vol.1(1): 39–59. http://dx.doi.org/10.18063/SOM.2016.01.004.

1. Introduction

Circulation and hydrography over coastal and shelf waters of Nova Scotia have significant temporal and spatial variability. For instance, sharp sea surface temperature fronts were observed along the coast of Nova Scotia on September 1, 2012 by the Moderate Resolution Imaging Spectro-radiometer (MODIS) instrument onboard the Aqua satellite (Figure 1). The main physical processes that affect circulation, hydrography and associated variability over the Scotian Shelf (SS) and adjacent waters include tides, net heat and freshwater fluxes at the sea surface, shelf-slope exchange, freshwater runoff, and other atmospheric forcing. The tides along the south shore of Nova Scotia are mainly semi-diurnal with amplitudes of the M_2 constituent increasing from ~50 cm at the northeast tip to ~100 cm at the southwest tip of Nova Scotia (Dupont, Hannah, Greenberg *et al.*, 2002). In the Bay of Fundy (BoF), the tides resonate significantly with local geometry (Garrett, 1972) to produce a large (up to ~17 m) tidal range at the head of the BoF. Associated with large tides, strong tidal currents in the BoF provide an effective mechanism to vertically mix the water column (Garrett, Keeley and Greenberg, 1978).

The sea surface temperature (SST) over the study region has a strong seasonal cycle, with a mean range of about 16°C (Thompson, Loucks and Trites, 1988), largely due to the intense negative and positive heat fluxes at the sea surface from the atmosphere to the ocean in winter and summer respectively. The interannual

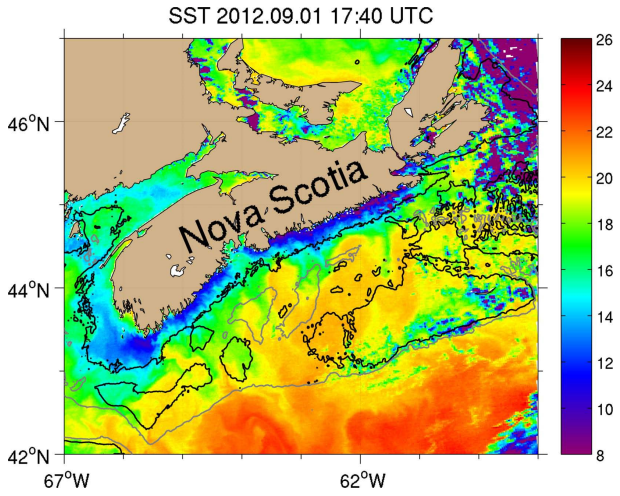

Figure 1. MODIS satellite remote sensing sea surface temperature (SST) on September 1, 2012. Data extracted from the Ocean Color Website (http://oceancolor.gsfc.nasa.gov). The 100 m and 200 m isobaths are shown in black and gray contours, respectively.

and decadal variability of temperature and salinity on the SS is affected significantly by variations of the westward transport of the Labrador Current through the shelf-slope exchange (Petrie and Drinkwater, 1993). The freshwater discharge from the St. Lawrence River (SLR) also plays an important role in affecting the salinity and circulation in the Gulf of St. Lawrence-Scotian Shelf-Gulf of Maine (GSL-SS-GoM). Previous studies suggested that the freshwater discharge signal of the SLR from Québec City reaches Halifax and Cape Sable in about 6 months (Sutcliffe, Loucks and Drinkwater, 1976) and about 8–9 months (Smith, 1989), respectively.

The general circulation on the SS is characterized by southwestward (equatorward) currents with inshore and offshore branches (See Loder, Petrie and Gawarkiewicz (1998) for a detailed review). The inshore branch is the Nova Scotia Current, which originates in the GSL. This current turns onto the SS at Cabot Strait and drifts southwestward along the coast of Nova Scotia and enters the GoM at Cape Sable ("1" in Figure 2B). The offshore branch represents a downstream extension of the Labrador Current, which is the subpolar western boundary current in the northwest Atlantic. The offshore branch of the Labrador Current reduces its transport while flowing along the shelf break of the SS and entering the GoM through the Northeast Channel (Hannah, Shore, Loder *et al.*, 2001; Han and Loder, 2003). The climatological flow over the SS outlined above generally persists year-round, but with strong seasonal variations in the transport on the inner shelf and at the shelf edge. Both the Nova Scotia Current and the shelf break current are thought to be strongest in winter and weakest in summer (Loder, Hannah, Petrie *et al.*, 2003). In addition to the alongshore currents, the onshore flow of the nutrient-rich Slope Water occurs in several major cross-shelf channels (e.g., Laurentian Channel, Scotian Gulf and Northeast Channel (Smith, Houghton, Fairbanks *et al.*, 2001), see Figure 2B).

Wind stress and associated variability also play an important role in driving the circulation and hydrography variation of Nova Scotia's coastal and shelf waters. The dominant southwesterly wind in summer on the SS is favorable for coastal upwelling. Based on satellite images, Petrie, Topliss and Wright (1987) demonstrated the development of a band of cool water over the inner SS during a month-long period of upwelling-favorable winds in 1984. In addition, tropical and winter storms can generate significant storm surges, shelf waves, and intense inertial currents on the SS and adjacent waters (Sheng, Zhai and Greatbatch, 2006).

With the advent of computer technology and significant progress in numerical methods in the last 50 years, numerical ocean circulation models have increasingly been used in simulating three-dimensional (3D) circulation and hydrography in the ocean. Various numerical models were developed for simulating the circulation and hydrography of Nova Scotia's coastal and shelf waters (Urrego-Blanco and Sheng, 2014; Thompson, Ohashi, Sheng *et al.*, 2007; Wu, Tang and Hannah, 2012). One of these numerical models is a 3D ocean circulation modelling system known as DalCoast. DalCoast has been developed over the past two decades to simulate circulation and hydrography for the GSL-SS-GoM region. The earliest version of this model was used to simulate the storm surge and two-dimensional (2D) circulation over the eastern Canadian shelf with a special emphasis on the SS and GSL region (Bobanovic, 1997). An improved version was then applied to simulate 3D circulation and hydrography over the coastal and shelf waters of Nova Scotia (Thompson, Ohashi, Sheng *et al.*, 2007), using a simple data assimilation method known as spectral nudging to suppress seasonal bias and drift in the model. A more recent version was further developed with important modifications including an enlarged model domain and higher resolution atmospheric forcing (Ohashi and Sheng, 2013). A multi-nested version of DalCoast was developed by Yang and Sheng (2008)

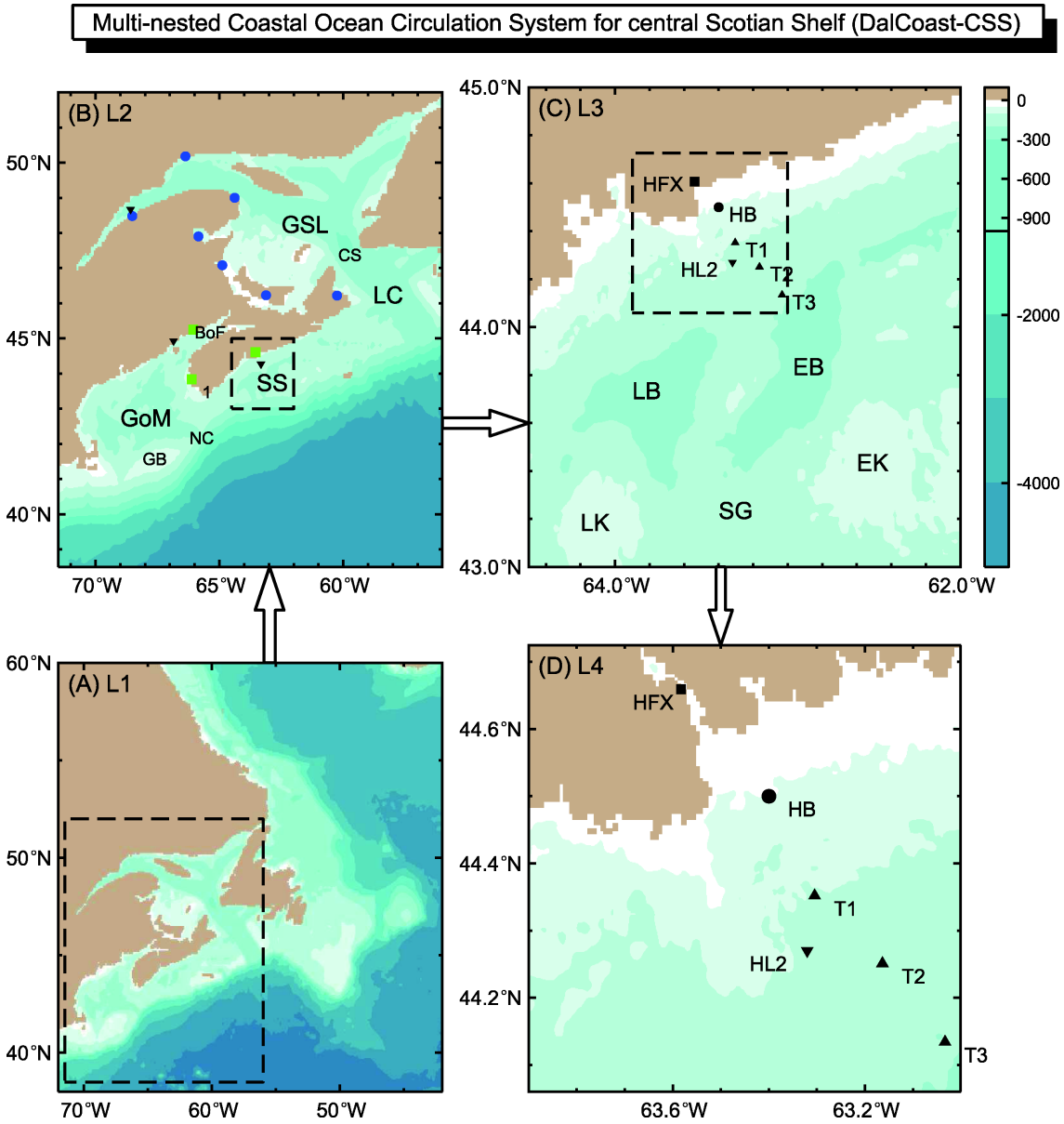

Figure 2. Domains and major bathymetric features of the four submodels of the nested-grid ocean circulation model. In (B), the blue solid circles and green solid squares indicate the tide gauge locations; the downward-pointing triangles indicate the position of hydrographic stations: Rimouski in the GSL, Station 2 on the SS, and Prince 5 in the BoF. In (C) and (D), the black solid circle indicates the position of the marine buoy outside Halifax Harbour (HB); the black solid square indicates the position of the tide gauge in Halifax Harbour (HFX); the black upward-pointing triangles indicate positions of three current moorings: T1, T2 and T3; the black downward-pointing triangle indicates the position of Station 2 (HL2). Land is marked by the tan color. The Gulf of Maine (GoM), Scotian Shelf (SS), Gulf of St. Lawrence (GSL), Bay of Fundy (BoF), Northeast Channel (NC), Laurentian Channel (LC), Cabot Strait (CS) and Georges Bank (GB) are labelled in (B). In (B), "1" represents Cape Sable. LaHave Basin (LB), LaHave Bank (LK), Emerald Basin (EB), Emerald Bank (EK) and Scotian Gulf (SG) are labelled in (C).

and later by Shan *et al*. (2011). DalCoast has been applied using a one-way nesting technique to simulate circulation and hydrography over three scientifically and socio-economically important marine areas of Nova Scotia: Lunenburg Bay (DalCoast-LB, Yang and Sheng, 2008), Halifax Harbour (DalCoast-HFX, Shan, Sheng, Thompson *et al*., 2011) and Sable Gully (DalCoast-Gully, Shan, Sheng and Greenan, 2014). Circulation and hydrography simulated by the multi-nested version of DalCoast were extensively validated against observations (Yang and Sheng, 2008; Shan, Sheng, Thompson *et al*., 2011, Shan, Sheng and Greenan,

2014).

However, it is a great challenge for a numerical model to accurately reproduce the observed circulation and associated variability over the coastal and shelf waters of Nova Scotia, including the above-mentioned observed SST fronts and the Nova Scotia Current, since many important physical processes in operation are not fully understood. For example, what are the variations in the strength and offshore extension of the SST front? What are the main physical factors affecting the interannual variability of the Nova Scotia Current? How is the circulation over the SS affected by the Slope Water intrusion? The main objective of this study is to assess the performance of a nested-grid model for the coastal and shelf waters of Nova Scotia by using satellite remote sensing data and in situ oceanographic observations. This paper presents the latest version of DalCoast to date, in which the domain of the finest-resolution (~500 m) submodel covers the inshore part of the central SS region extending about 200 km seaward from Halifax Harbour and passing Emerald Basin to the shelf break (Figure 2). The nesting approach provides a computationally efficient method to better resolve physical processes over the central SS, such as the Nova Scotia Current, coastal upwelling and shelf-slope exchange, within the upstream and downstream regions.

In section 2, the nested-grid circulation model is described. In section 3, the model performance is assessed by comparing against various observations. In section 4, the nested-grid model is used in a process study to quantify the major processes affecting the cold surface water formation along the Nova Scotia coast in summer. A summary is presented in the last section.

2. Circulation Model and Forcing

The nested-grid ocean circulation modelling system used in this study consists of four submodels, with progressively smaller model domains and finer horizontal resolutions zooming from the northwest Atlantic into the central SS. The two outermost submodels, L1 and L2, are based on the Princeton Ocean Model (POM, Mellor, 2004). Submodel L1 is a 2D barotropic storm surge model covering the eastern Canadian shelf from the Labrador Shelf to the GoM with a horizontal resolution of 1/12°. Submodel L2 is a 3D baroclinic model covering the GSL, the SS, and the GoM with a horizontal resolution of 1/16° and 40 σ-layers in the vertical. Submodels L3 and L4 are also 3D and baroclinic with a horizontal resolution of ~2 km and ~500 m, respectively. Submodels L3 and L4 are based on the free-surface version of CANDIE (Sheng, Wright, Greatbatch *et al*., 1998), which is a 3D primitive-equation ocean circulation model that uses the A-grid, z-levels in the vertical and a fourth-order advection scheme. There were 47 z-levels in the vertical in submodels L3 and L4, with relatively fine vertical resolutions of 3 m in the first layer, and 4 m between 3 m and 103 m, and 8 m in the deep water. The one arc-minute interval gridded bathymetry data from GEBCO (www.gebco.net) is used for the model bathymetry. This new version of DalCoast is called DalCoast-CSS.

The horizontal subgrid-scale mixing parameterization in DalCoast-CSS (L1 to L4) is based on the shear- and grid-size dependent scheme of Smagorinsky (1963). The vertical subgrid-scale mixing parameterization in submodels L2 is based on the Mellor and Yamada (1982) level-2.5 turbulent closure scheme, while an enhanced version of the K profile parameterization (KPP) scheme (Durski, Glenn and Haidvogel, 2004) is used in submodels L3 and L4.

Monthly-mean temperature and salinity climatology (Geshelin, Sheng and Greatbatch, 1999) with a horizontal resolution of 1/6° is used in initializing submodels L2, L3 and L4. The temperature and salinity in the model are spectrally nudged toward the seasonal-mean climatologies at depths greater than 40 m in submodels L2 and L3 using the spectral nudging method (Thompson, Ohashi, Sheng *et al*., 2007). Hence, the model temperature and salinity in the top 40 m evolve freely under the influence of external forcing. In addition, the semi-prognostic method (Sheng, Greatbatch and Wright, 2001) is used to further reduce the seasonal drift in the simulated circulation in submodel L2. In this method, the simulated density in the hydrostatic equation is expressed as a linear combination of the simulated density and the climatological density, which is equivalent to adding a correction term to the horizontal pressure gradient terms in the momentum equation (Sheng, Greatbatch and Wright, 2001).

The nested-grid modelling system is driven by atmospheric forcing, heat fluxes, freshwater input and lateral open boundary conditions. The atmospheric forcing includes three-hourly sea level pressure (SLP) and surface wind fields taken from the North American Regional Reanalysis (NARR) with a horizontal resolution of ~32 km (Mesinger, DiMego, Kalnay *et al*., 2006). The bulk formula suggested by Large and Pond (1981) and modified by Powell, Vickery and

Reinhold (2003) is used to convert the wind speed to wind stress. The NARR wind stress and SLP fields are linearly interpolated to every model timestep and mapped to each model grid.

The net heat fluxes at the sea surface used to drive submodels L2, L3 and L4 are calculated using the three-hourly NARR reanalysis fields of the air temperature, relative humidity, cloud cover, air pressure, and wind speed. Freshwater inputs from major rivers in the region are implemented in submodel L2 using idealized channels cut into the model's coastline. A simple numerical scheme based on the salt and volume conservation is used in the model to specify salinity and surface elevation at the head of each idealized channels (see Ohashi and Sheng (2013) for details).

The lateral open boundary conditions used in submodel L2 include the specification of surface elevations and depth-averaged currents at the open boundaries. At the eastern open boundary, for example, the modelled normal flow (u_e) and surface elevation (η_e) take the following relationship (Flather and Davies, 1976):

$$u_e = u_c + u_w + u_t + \frac{c}{h}(\eta_e - \eta_w - \eta_t) \qquad (1)$$

where η_w is the wind-driven surface elevation calculated by submodel L1, η_t is the hourly tidal sea surface elevation which is calculated by using harmonic constants extracted from the TPXO tidal model (Egbert and Erofeeva, 2002) for the eastern continental shelf of North America for eight major tidal constituents (M_2, S_2, N_2, K_2, K_1, O_1, P_1 and Q_1). A detailed description of the TPXO tidal model and extraction method can be found at http://volkov.oce.orst.edu/tides/EC.html. In Equation 1, u_w and u_t are the depth-averaged wind-driven and tidal currents from submodel L1 and TPXO, respectively, u_c is the climatological daily-mean baroclinic currents (temporally interpolated from five-day means) produced by a coarse-resolution circulation model for the northwest Atlantic Ocean (Urrego-Blanco and Sheng, 2012), c is the phase speed of the external gravity wave, and h is the local water depth.

The lateral open boundary conditions for submodels L3 and L4 are based on the following one-way nesting technique. The Orlanski (1976) radiation condition is first used to determine whether the propagation direction at the finer-resolution domain's open boundary is inward or outward. For inward propagation, model variables (i.e., temperature, salinity, and normal flow) of finer-resolution domains at the open boundary are restored to the model results produced by the larger domain upper-level submodels, with a restoring timescale of 12 hours for normal flow and 15 days for temperature and salinity. For outward propagation, the model variables of the inner model at the open boundary are radiated outward. An inverse distance-weighted interpolation is used to map the σ-layer results in submodel L2 onto the z-level points of the lateral open boundary in submodel L3. Since submodels L3 and L4 have a common vertical configuration, only horizontal interpolations are performed along the open boundaries of submodel L4.

3. Model Validation

DalCoast-CSS is initialized from the January mean hydrographic climatology and integrated from a state of rest for two years from January, 2011 to the end of 2012 using the configuration described in section 2. In the model assessment, we mainly focus on the model results for 2012. The oceanographic measurements used for the assessment include satellite remote sensing data from GHRSST and Aquarius, and in situ oceanographic observations made by tide gauges, a marine buoy, ADCPs and CTDs.

3.1 Sea Level

Sea level observations are made by tide gauges at several locations in the study region (Figure 2B). A MATLAB package known as T_TIDE (Pawlowicz, Beardsley and Lentz, 2002) was used to conduct harmonic analysis of observed and simulated sea levels. Ohashi and Sheng (2015) recently assessed the performance of submodel L2 in simulating tides in the GSL. In this study, we assess the model performance in simulating tides in the GSL-SS-GoM region. Figure 3 shows scatterplots between the observed and simulated amplitudes and phases of tidal elevation for the M_2 and K_1 constituents for 2012 at 10 tide gauge locations. The following index (Thompson and Sheng, 1997) is used to provide a quantitative measure of the model performance,

$$\gamma^2 = \frac{Var(O-M)}{Var(O)} \qquad (2)$$

where *Var* represents the variance operator, and O and M denote the observed and model simulated variables respectively. The smaller γ^2 is, the better the performance of the model is. Empirically, the threshold value of γ^2 is chosen to be 1. The calculated γ^2 is relatively

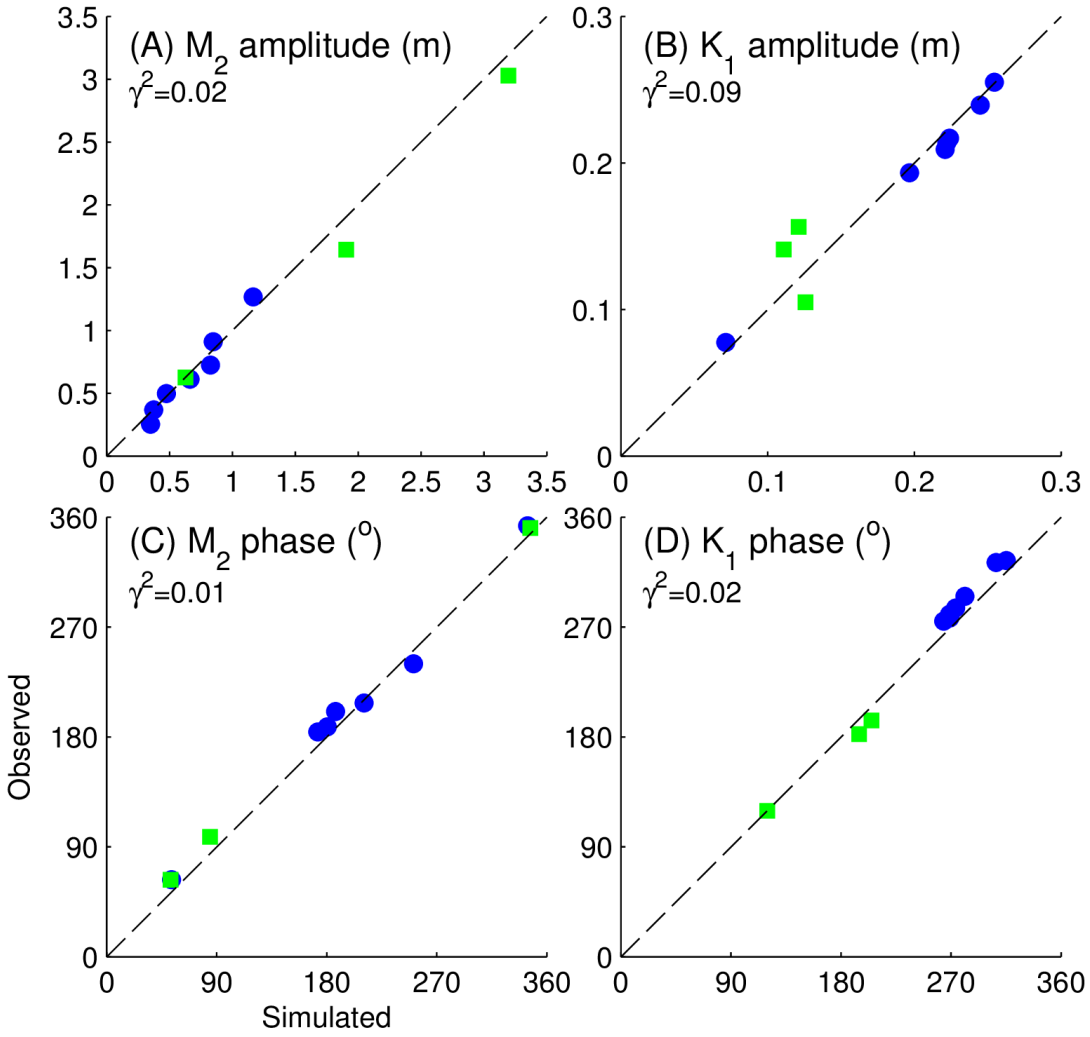

Figure 3. Scatterplots between observed and simulated amplitudes and phases of tidal elevations for the M_2 and K_1 tidal constituents for 2012 at 10 tide gauge locations shown in Figure 2B. Stations in the Gulf of St. Lawrence are shown in circles. Outside the Gulf, the stations are shown in squares.

small (< 0.1) and similar to the previous results (Ohashi and Sheng, 2015), indicating that submodel L2 is able to capture the tides in the GSL-SS-GoM region.

We next assess the performance of the innermost submodel L4 in simulating tidal and non-tidal components of sea levels in Halifax Harbour. Sea level observations have been made at a tide gauge in Halifax Harbour for almost a century (see the position marked by a black square in Figure 2C). Observations of sea levels in a 2-month period (November 1 to December 31, 2012) at Halifax Harbour demonstrate that sea levels are strongly affected by tides which are predominantly semi-diurnal (Figure 4A). A pronounnced spring and neap variation is also evident in the sea level observations mainly due to the beating of the M_2 and S_2 tidal constituents. From the neap to spring tide, the observed tidal range increase from about 0.6 to 2.0 m. Non-tidal components of observed sea levels (Figure 4B), which include the storm surge and inverse barometer effect ($\eta_a = -\tilde{P}_a / \rho g$, where $\tilde{P}_a$ is the atmospheric pressure perturbation, ρ is the density of seawater and g is the acceleration of gravity), also contribute to the total sea level variations. Several peaks in the observed non-tidal component (Figure 4B) can be seen in fall and winter associated with storm events. Non-tidal observed sea levels are relatively small in summer due mainly to less severe weather conditions over the study region in summer than in other three seasons.

Overall, submodel L4 reproduces very well the sea level observations (Figure 4A and B). The simulated

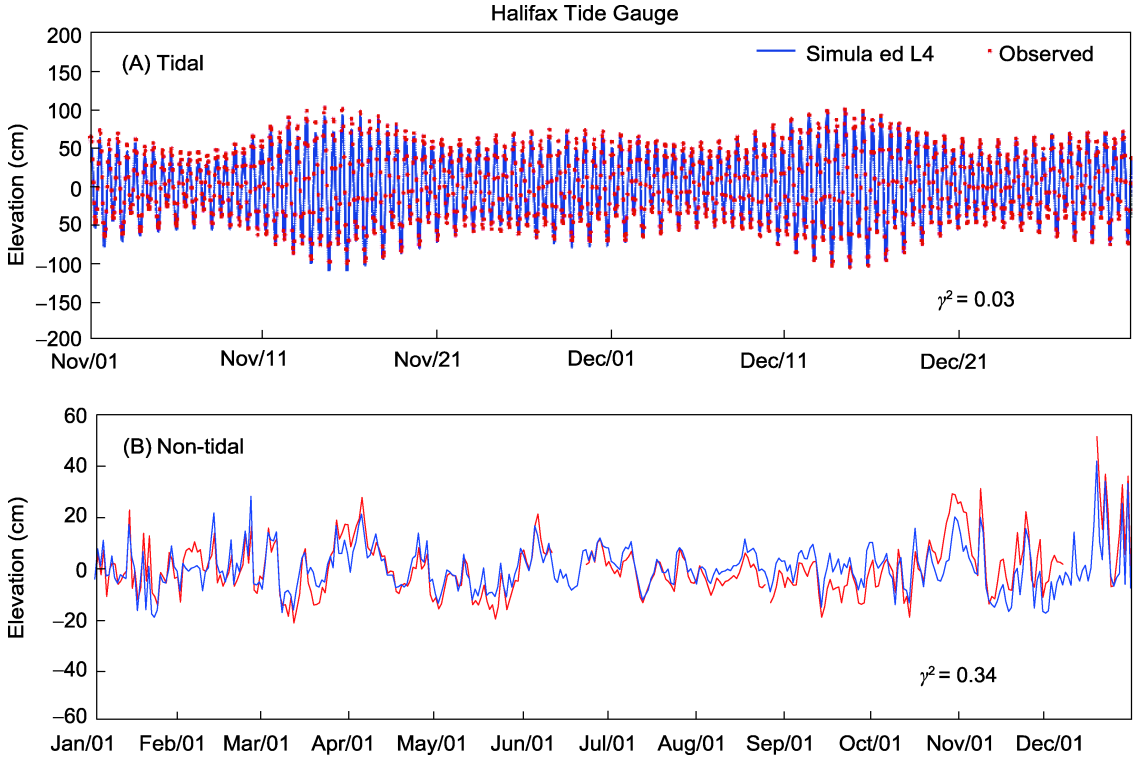

Figure 4. Time series of observed (red) and simulated (blue) (A) tidal and (B) non-tidal sea surface elevations at a tide gauge in Halifax Harbour (CHS 490). The simulated results are produced by submodel L4. The observed and simulated sea surface elevations are decomposed into tidal and non-tidal components using the MATLAB package T_TIDE.

tidal component is in good agreement with observations both in amplitudes and phases. The simulated non-tidal component is in reasonable agreement with the observations except for large mismatches during several occasions, mainly due to the less accurate atmospheric forcing during strong storm events used in driving the model. We found γ^2 = 0.03 for tides and γ^2 = 0.34 for non-tidal components at Halifax Harbour in 2012. These low values of γ^2, which are similar to those discussed in previous studies (Shan, Sheng, Thompson *et al.*, 2011), indicate that DalCoast-CSS performs well in simulating sea level variability in Halifax Harbour at timescales of hours to seasons.

3.2 Hydrography

We next evaluate the performance of DalCoast-CSS in simulating 3D hydrography. Temporal evolution of hydrography produced by the model is affected by both internal dynamics of the model and external forcing at the sea surface and along model open boundaries. The focus of this section is on the assessment of the model performance in simulating hydrography in the upper ocean, where the spectral nudging method was not applied in the model.

(a) Satellite Remote Sensing Observations

SEA SURFACE TEMPERATURE (SST): The simulated SST produced by submodel L2 of DalCoast-CSS has significant seasonal variations (Figure 5A). In February, the SST is relatively cold (~0°C) in the shelf water region, including the GSL, SS and GoM; and relatively warm (~15°C) in the Slope Water region and adjacent deep waters. In May, the SST on the shelf starts to warm up to ~5°C. In August, the SST further increase to ~20°C in the shelf water region and ~25°C in the deep water region, mainly due to the positive surface heat flux from the overlying atmosphere to the ocean. It should be noted that submodel L2 generate relatively cold surface waters in the Georges Bank, BoF and off Cape Sable due to the strong tidal mixing over the shallow banks. In November, the simulated SST decreased to ~15°C on the shelf water region and ~20°C in the deep water region.

The satellite remote sensing SST data (Figure 5B) produced by the GHRSST (Group for High Resolution Sea Surface Temperature) Multiscale Ultrahigh Resolution (MUR) project (http://dx.doi.org/10.5067/GHGMR-4FJ01) are used to assess the model performance in simulating temporal and spatial variability of

SST in the study region. The global Level 4 (i.e., gridded and with gaps filled) GHRSST MUR SST has a horizontal resolution of 1-2 km, which is based upon nighttime GHRSST L2P skin and subskin SST observations from several instruments such as the NASA Advanced Microwave Scanning Radiometer-EOS (AMSRE), and the MODIS on the NASA Aqua and Terra platforms.

Figure 5C presents seasonal model biases in the SST, which are represented by differences between the simulated and observed monthly-mean SST. The seasonal biases of submodel L2 are relatively small and less than 2°C on the SS, indicating that DalCoast-CSS performs reasonably well in simulating the SST over this region. In the GoM, the model underestimates the SST in February by ~2°C and overestimates the SST in August and November by ~2°C. In the GSL, relatively large model biases occur over the western side in August and eastern side in November. In addition, the model has a deficiency in simulating the warm core ring detachment observed in the Slope Water region (Figure 5B-2). The major reason for this model deficiency is that the current, temperature and salinity at the open boundaries of submodel L2 are climatological five-day means produced by a coarse-resolution model for the northwest Atlantic Ocean (Urrego-Blanco

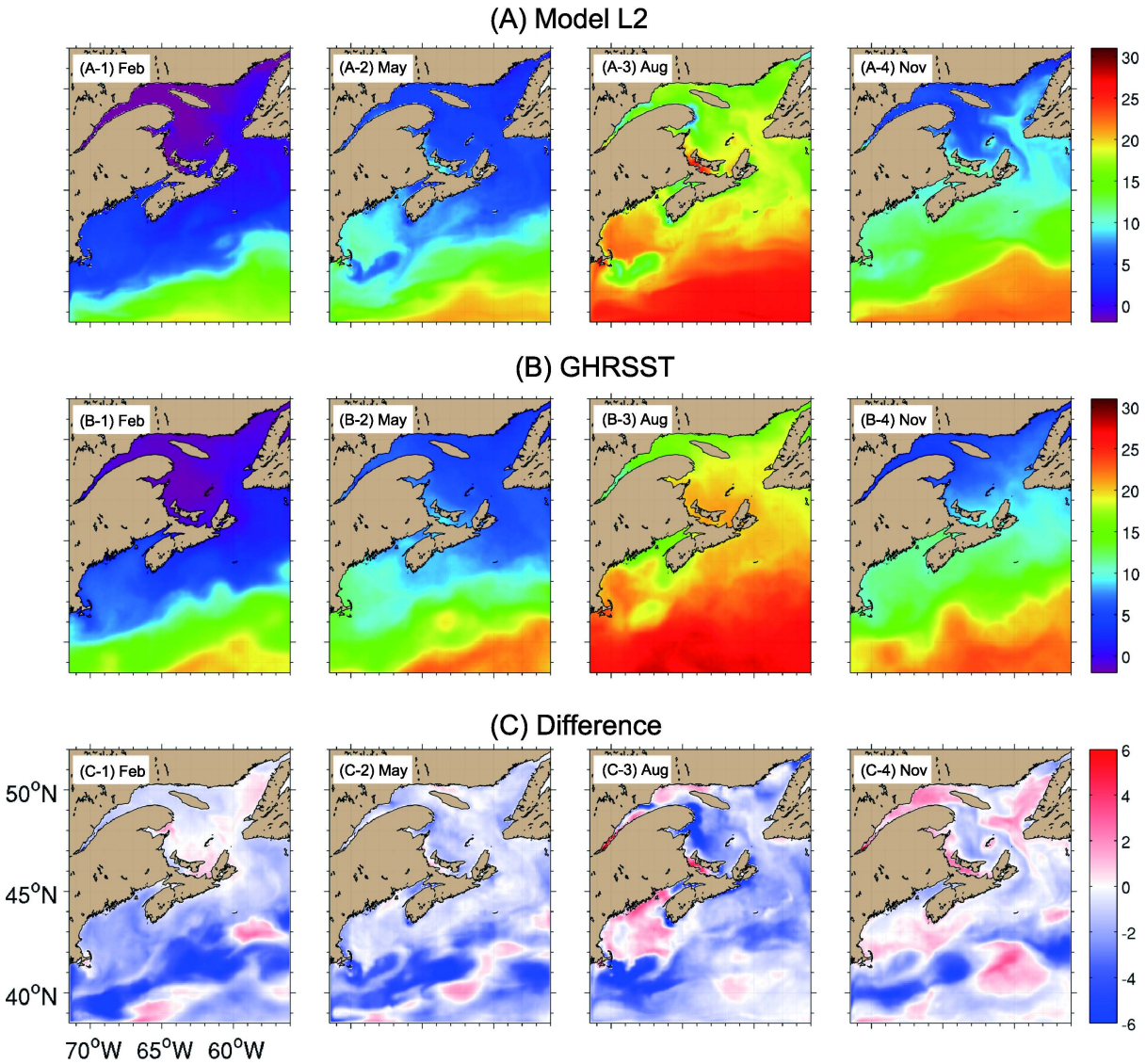

Figure 5. Simulated (upper panels) and observed (middle) monthly-mean sea surface temperature (SST) fields (in °C) in February, May, August and November 2012. Lower panels present the model biases represented by differences between the simulated and observed monthly-mean SST in each month. The simulated results are produced by submodel L2. The observations are extracted from the GHRSST MUR Level 4 product(http://dx.doi.org/10.5067/GHGMR-4FJ01).

and Sheng, 2012). As a result, without data assimilation, it is very difficult for DalCoast-CSS to realistically reproduce the timing and location of detachment of warm-core rings in the Slope Water region.

SEA SURFACE SALINITY (SSS): The simulated SSS produced by submodel L2 of DalCoast-CSS is presented in Figure 6A. The model generates a sharp shelf-slope salinity front marked by the 34 psu contour (Figure 6A) over the Slope Water region off the SS and GoM in February, May, August and November. Another noticeable feature in the simulated SSS is the low-salinity surface waters in the western GSL, along the south shore of Nova Scotia, and over the northeastern GoM (Figure 6A). These low-salinity waters have significant seasonal variations due to the time-varying freshwater discharge from the SLR. In spring, SLR runoff specified in the model increases significantly due to the melting of ice and snow. As a consequence, the simulated SSS decreases in the northwestern GSL in May. In August, the simulated SSS in the western GSL further decreases and the low-salinity surface water extends offshore along the Laurentian Channel to reach the shelf break. In November, the simulated SSS decreases along the south shore of Nova Scotia. In February, the simulated SSS decreases in the western SS and the eastern GoM. The propagation of a

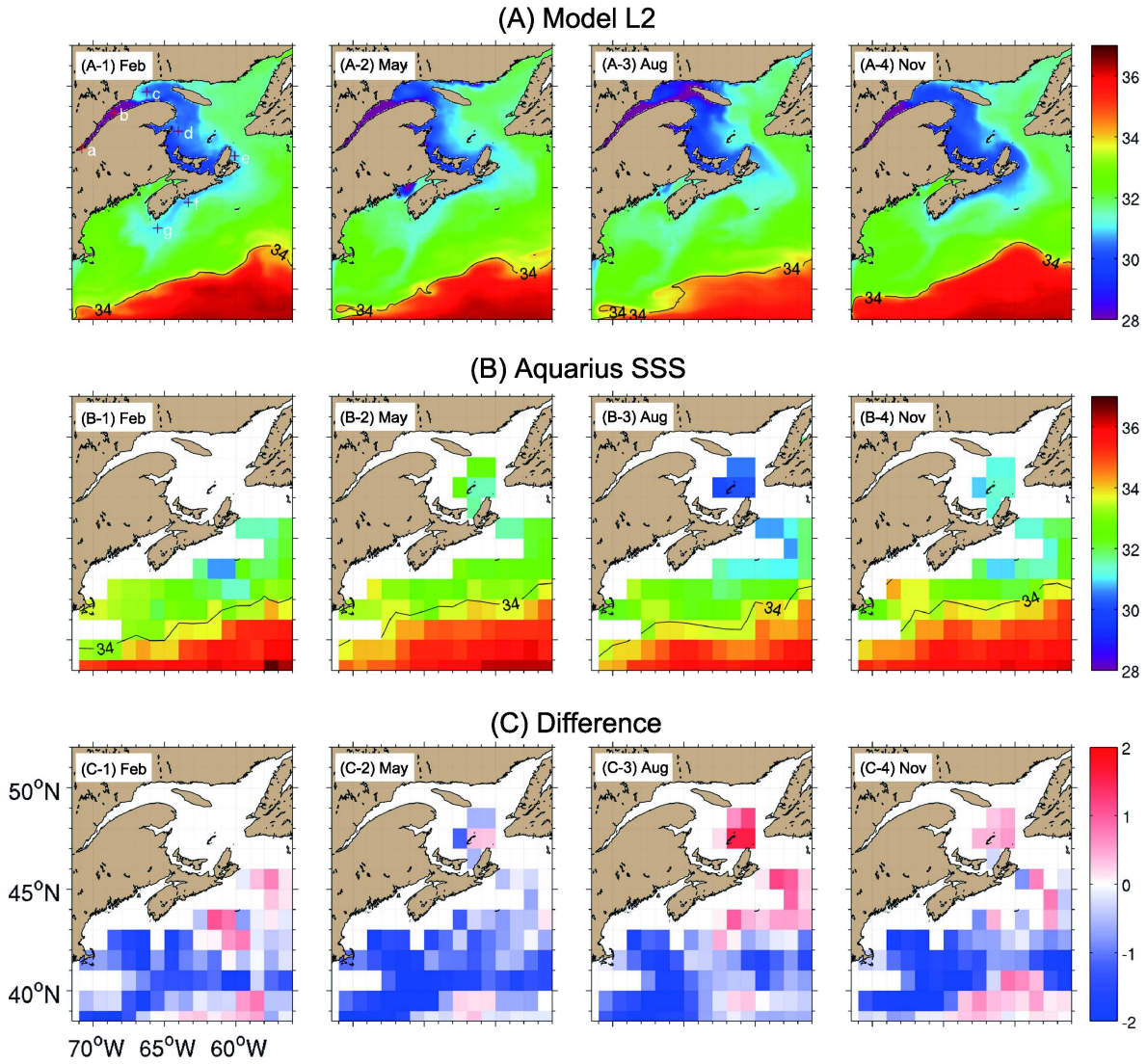

Figure 6. Simulated (upper panels) and observed (middle) monthly-mean sea surface salinity (SSS) fields in February, May, August and November 2012. Lower panels present model biases represented by differences between the simulated and observed monthly-mean SSS in each month. The simulated results are produced by submodel L2. The observations are extracted from the Aquarius Level 3 sea surface salinity version 4 product. The locations marked by "+" in (A-1) are used in the discussion of freshwater pulse.

spring freshwater pulse of the SLR can be estimated from the time series shown in Figure 7. A discharge peak is followed by the downstream reduction of the amplitude and phase propagation of a low-salinity signal. The travel time of the freshwater pulse from Québec City is about 7 months and about 8 months to reach Halifax and Cape Sable, respectively. These estimated travel times are consistent with the values discussed in previous studies (Sutcliffe, Loucks and Drinkwater, 1976; Smith, 1989). The seasonal variations of SSS outside the mouth of the Saint John River (SJR) are also captured by the model in the BoF. A low-salinity SJR plume is evident in May due to the large freshwater discharge. The SJR plume decays in the following months due to the decrease in freshwater discharge of the SJR and strong tidal mixing in this region.

The satellite Aquarius SSS product (NASA Aquarius project, 2015) is used to assess the model performance in simulating the temporal and spatial variability of SSS in the study region. The Aquarius SSS was inferred from brightness temperatures at the sea surface measured by three satellite radiometers and can be considered approximately as the observed SSS in the top 1 mm of the ocean water. The Aquarius SSS data were available from August 2011 to June 2015 and not available after this period due to an unrecoverable hardware failure, which caused the termination of the mission. The latest (version 4) Aquarius Level 3 SSS

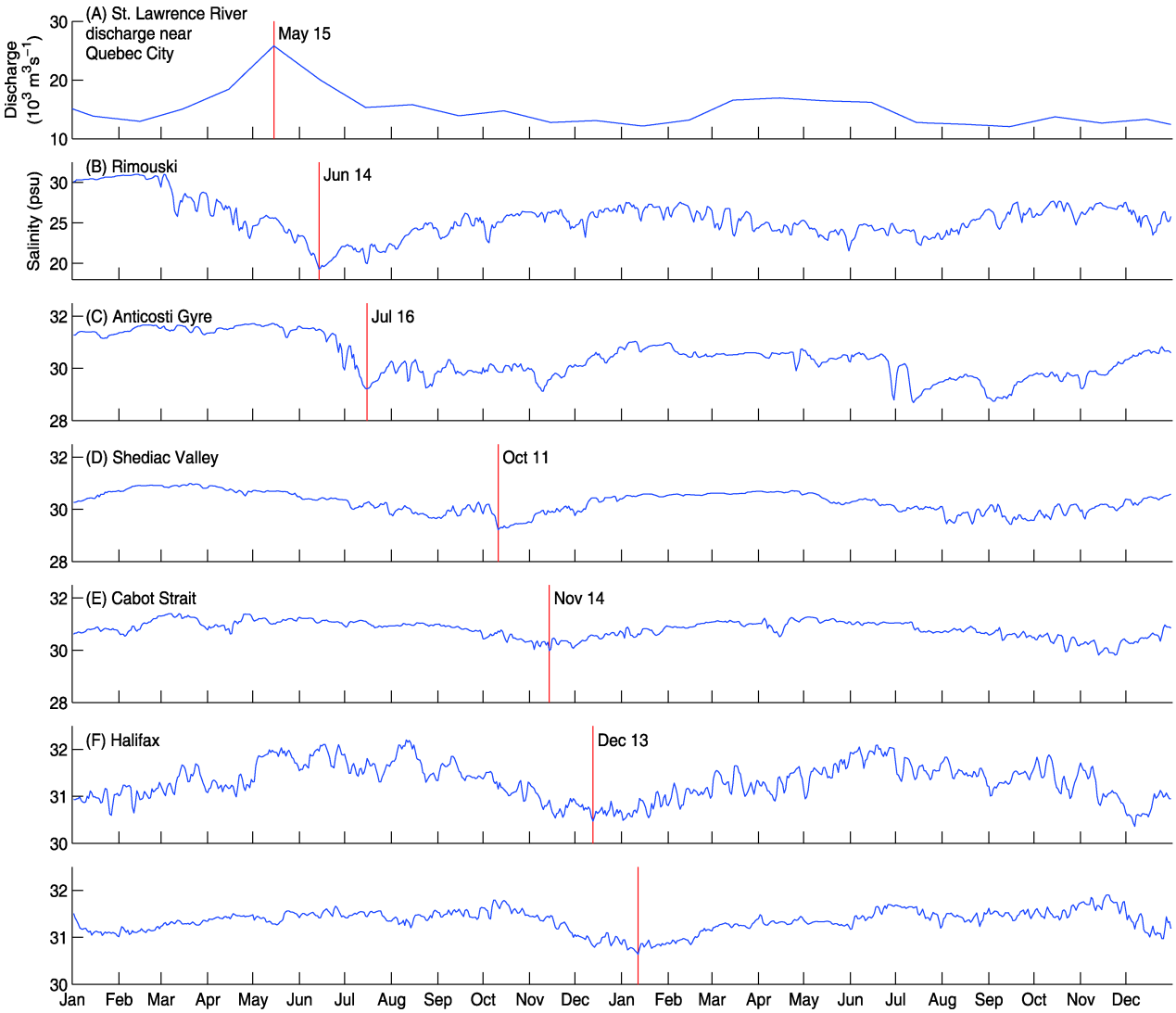

Figure 7. Time series of (A) the St. Lawrence River discharge near Québec City specified in the submodel L2 and (B-G) simulated sea surface salinity at selected downstream locations produced by submodel L2. The locations are marked by "+" in Figure 6 (A-1). The St. Lawrence River discharge maximum in 2011 is indicated by the red vertical line in (A) and the subsequent sea surface salinity minimum at selected downstream locations is also indicated by the red vertical line in (B-G).

product contains globally gridded 1 degree spatial resolution SSS. It should be noted that the Aquarius SSS is not available near the coast due to land contamination. The Aquarius SSS features large-scale patterns of seasonal variations in SSS over the GSL and on the SS (Figure 6B). In the interior of the GSL, the Aquarius SSS is relatively low in August. Over the shelf break adjacent to the Sable Island, the Aquarius SSS is relatively high in May. A salinity front can be seen from the Aquarius SSS in Figure 6B between the shelf water and the Slope Water in the four months. It should be noted that the spatial resolution of the Aquarius SSS is too coarse to resolve the salinity features near the coast. By comparison, the horizontal resolution of submodel L2 is about 1/16°, which is capable of resolving more horizontal features of the SSS than the Aquarius product.

Seasonal model biases in the SSS, which are represented by differences between the simulated and Aquarius monthly-mean SSS, are small on the eastern SS in the four months, particularly in May (Figure 6C-2). Submodel L2, however underestimates the monthly-mean SSS over the southwestern part of the model domain throughout the year by ~2 psu and overestimates the SSS in the interior of GSL in August and November by ~2 psu. The model deficiency in simulating the SSS could be explained by the lack of precipitation and evaporation processes at the sea surface in the model. In addition, as mentioned above, the current, temperature and salinity at the open boundaries of submodel L2 are climatological five-day means produced by a coarse-resolution model for the northwest Atlantic Ocean (Urrego-Blanco and Sheng, 2012).

(b) In situ Observations

We next assess the model performance using in situ hydrographic observations. Sea surface temperatures have been measured at a marine buoy located outside Halifax Harbour since 2000 (black solid circle marked by HB in Figure 2C). The observed daily-mean SST (Figure 8) has significant variability on various timescales, with the seasonal cycle being the dominant. The observed SST time series also exhibit several rapid cooling in mid-July, near the end of August and mid-October in 2012. These SST cooling events are strongly correlated with upwelling-favourable alongshore winds. In comparison with the SST monthly climatology constructed from the entire 14-year observations (2000–2013, the black line with open circles in Figure 8), the SST in 2012 is warmer than in the normal year. This is consistent with the previous findings by Hebert *et al.* (2013), that the annual-mean ocean temperature at discrete depths from surface to bottom over the SS and GoM in 2012 is the warmest between 1970 and 2012.

The observed seasonal cycle of SST and some of the synoptic variations in 2012 are well captured by submodel L4 with γ^2=0.04 (Figure 8). The simulated

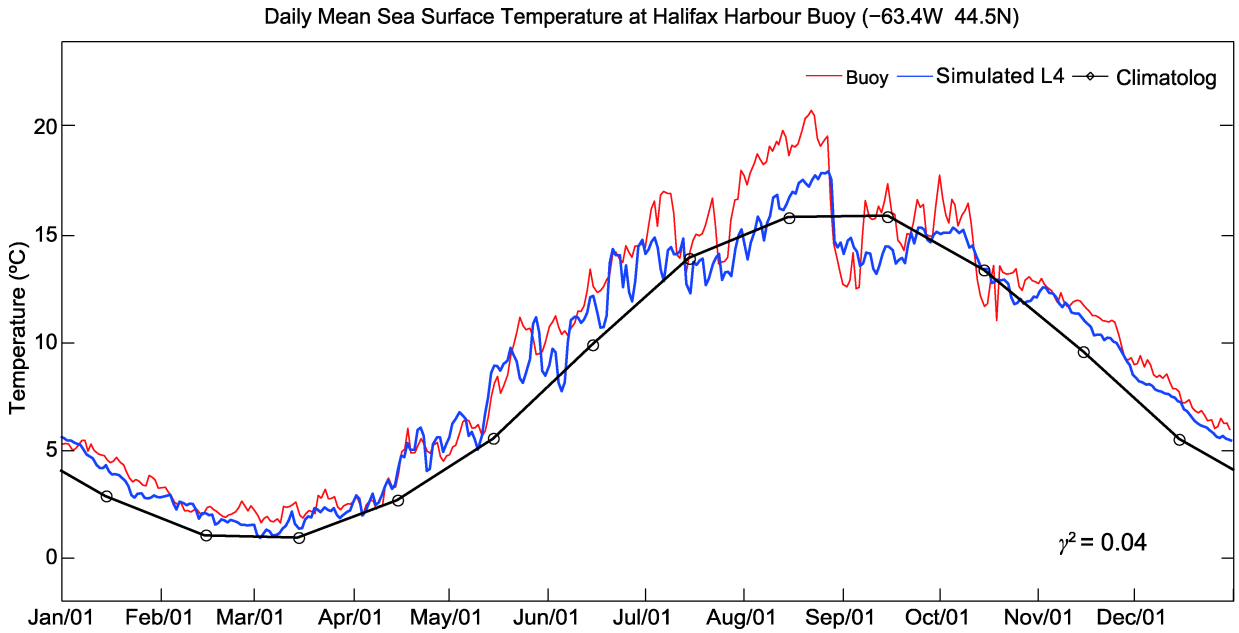

Figure 8. Time series of observed (red) and simulated (blue) sea surface temperature in 2012 at the marine buoy outside Halifax Harbour. The simulated results are produced by submodel L4.

SST in August increases with time, which is in good agreement with the observations, due mainly to the downward surface heat flux from the atmosphere to the ocean. The observed timing of the subsequent rapid cooling event at the end of August is well captured by the model, although the magnitude of the cooling is underestimated. It should be noted that the simulated SST is ~2°C cooler than the observed SST at the beginning of August and this model bias persists throughout the month of August for which the exact reason was unknown. One plausible explanation is the issue associated with the net heat flux calculation in the model. Figure 9 shows that the heat fluxes at the buoy location in the model are in the same order of magnitude as the heat fluxes provided by the NCEP Climate Forecast System Version 2 (CFSRv2) products (Saha, Suranjana, and Coauthors, 2011, updated monthly, 2016) with noticeable differences at high frequency. Another possible explanation is the crude vertical mixing parameterization used in the model.

The model performance in simulating the temperature and salinity in the water column is further assessed by comparing model results with CTD observations of temperature and salinity made by the Atlantic Zone Monitoring Program of Fisheries and Oceans Canada (Therriault, Petrie, Pepin *et al.*, 1998). Ohashi and Sheng (2015) recently validated the simulated temperature and salinity only in the GSL produced by a similar submodel L2. Here we focus on the validation by including observations made on the SS and in the BoF.

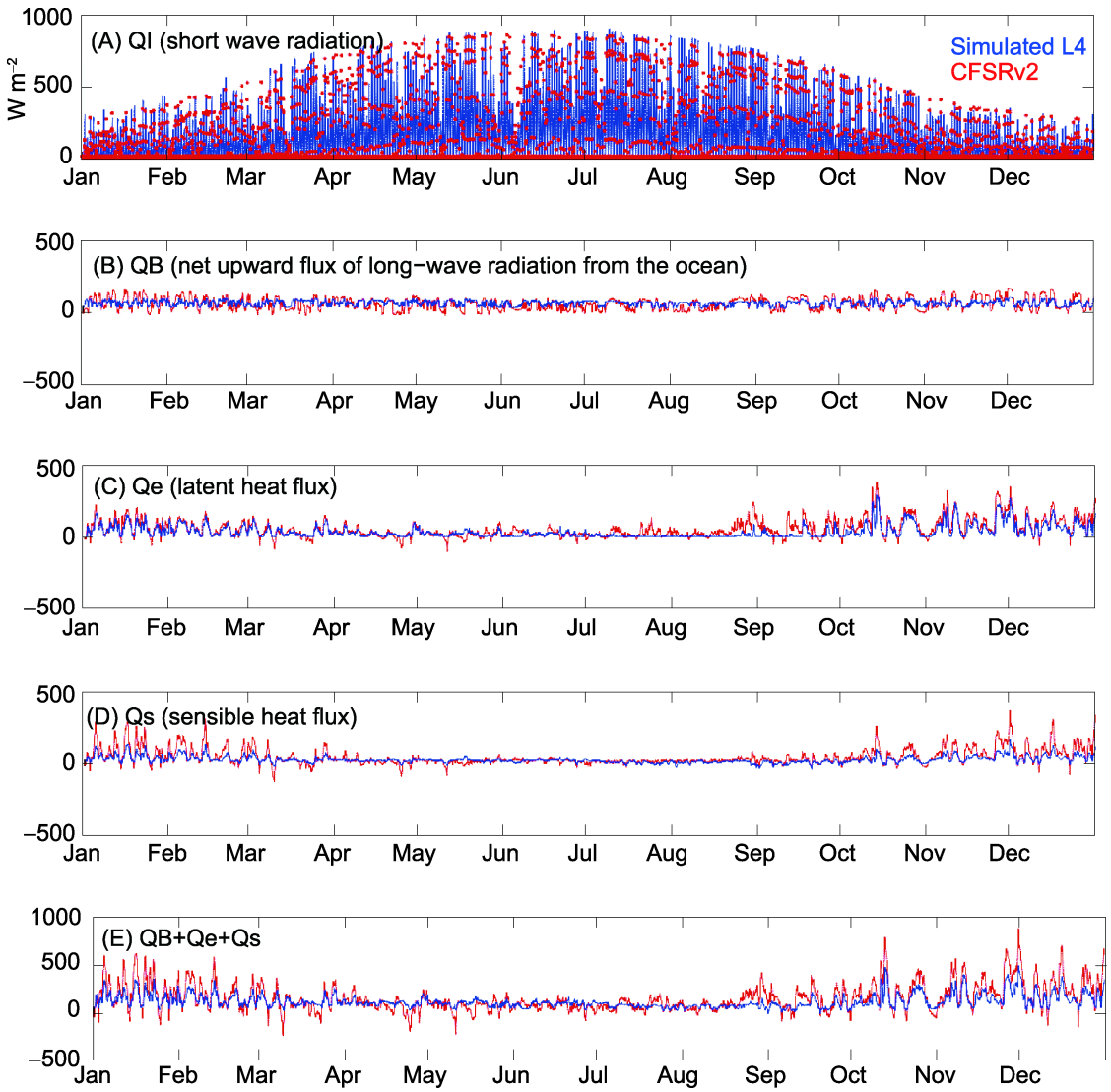

Figure 9. Time series of heat fluxes in 2012 produced by submodel L4 (blue) and CFSRv2 products (red) at the marine buoy outside Halifax Harbour.

Figure 10 shows scatterplots between temperature and salinity values simulated by submodel L2 for 2012 and their observed counterparts at Rimouski (in the GSL), Station 2 (on the SS) and Prince 5 (in the BoF). Calculated γ^2 values are similar to the values discussed by Ohashi and Sheng (2013, 2015), indicating that the current version of submodel L2 has a same level of performance in simulating the temperature and salinity in the study region.

The model performance in simulating the vertical distribution of temperature and salinity is assessed by comparing the innermost submodel L4 results with CTD observations of temperature and salinity made at Station 2 (downward-pointing triangle in Figure 2D) on the Halifax Line. Figure 11 presents a comparison between the simulated time-depth distribution of temperature and salinity produced by submodel L4 of Dal-Coast-CSS and the CTD observations at Station 2.

Submodel L4 is able to capture many observed features in the vertical temperature profiles at Station 2, including vertically uniform distributions in the top 60 m in late fall and winter and the development of

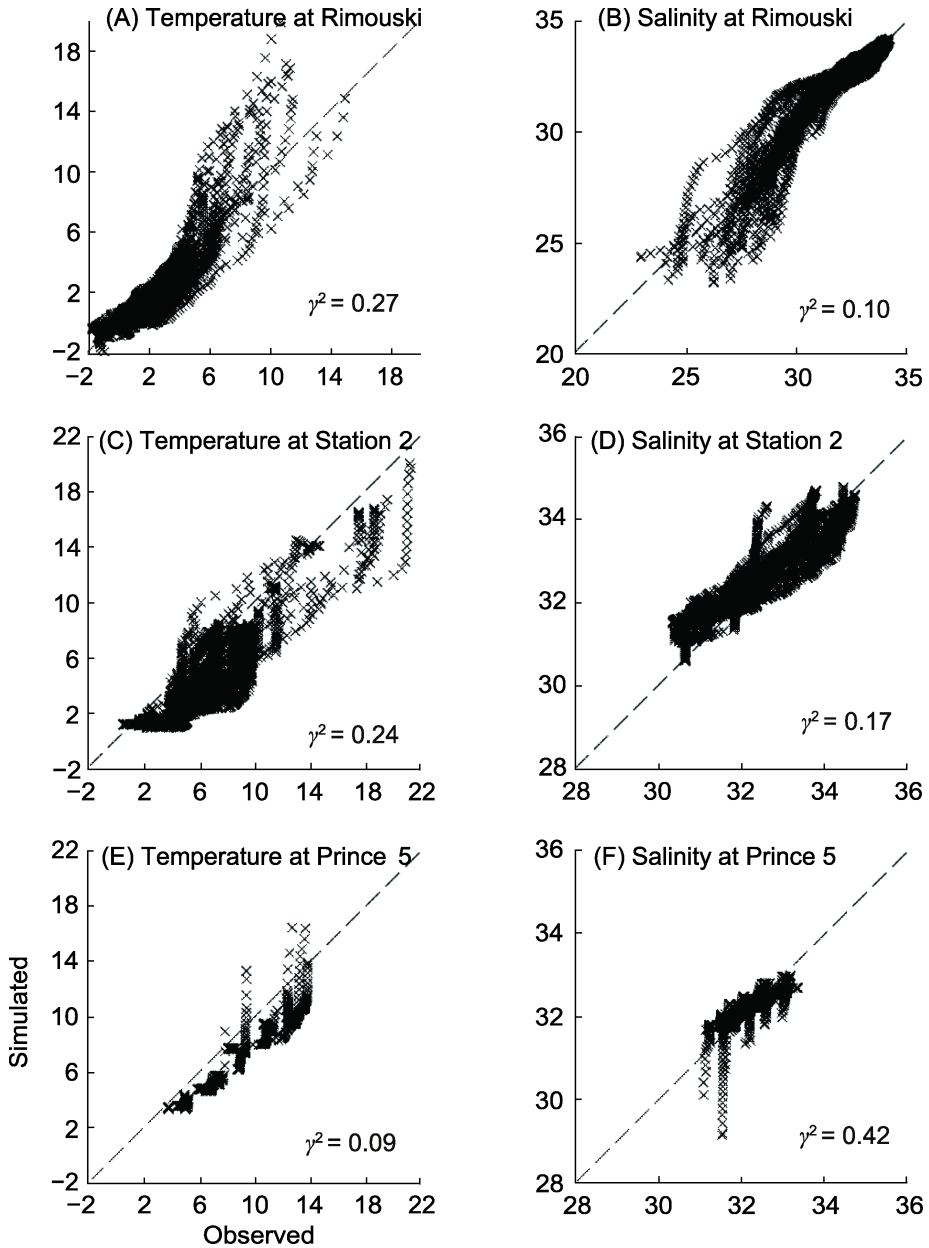

Figure 10. Scatterplots between observed and simulated temperature and salinity for 2012 at three hydrographic stations shown in Figure 2B: Rimouski in the GSL, Station 2 on the SS, and Prince 5 in the BoF.

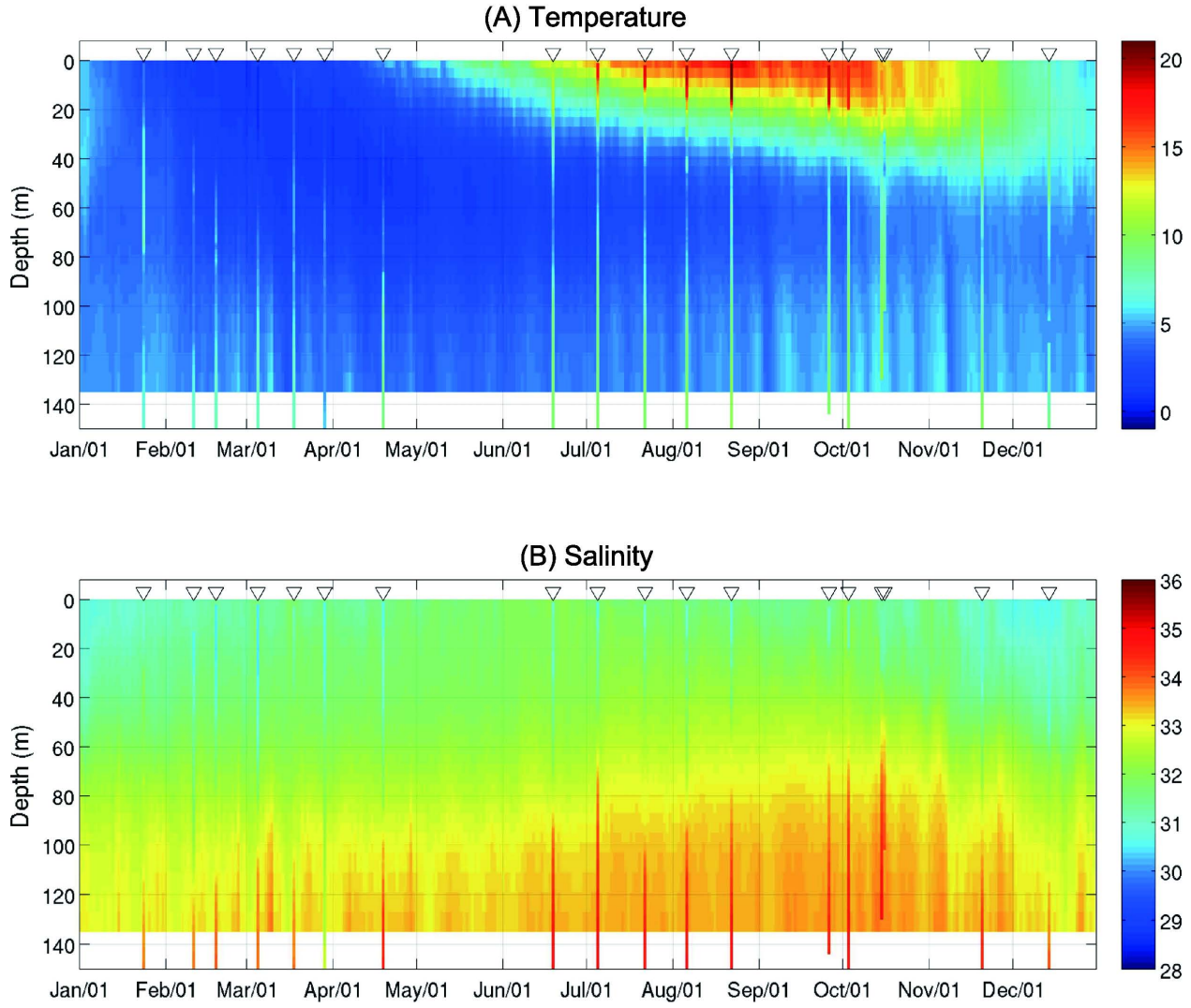

Figure 11. Time-depth distributions of simulated (A) temperature and (B) salinity at Station 2 in 2012. The simulated results are produced by submodel L4. The observed temperature and salinity profiles based on CTD casts are shown with 1-day width in the plots. The times of CTD casts are indicated by open triangles.

thermal stratification in summer (Figure 11A). The other important feature in summer reproduced by the model is the cold intermediate layer (CIL). The formation of the CIL is mainly due to winter convection, wind-induced mixing in the previous winter and advection of cold water by the Nova Scotia Current. The model is able to capture the three-layer vertical structure with a CIL in the middle of the water column in summer. However, the model overestimates the temperature in the CIL and underestimated the temperature in the top 20 m in comparison with the observed profiles in summer. We also compared the simulated heat fluxes at Station 2 with the heat fluxes provided by the NCEP Climate Forecast System Version 2 (CFSRv2) products and found no major differences. We speculated that model deficiency may be due to the crude vertical mixing parameterization used in the model.

The nested-grid model is also able to capture the general vertical structure in salinity at Station 2 (Figure 11B). The low salinity in the upper layer of ~40 m in late fall and winter at Station 2 of Halifax Line is associated with the arrival of the low-salinity water from the GSL. The model is also able to reproduce a bottom layer with relatively high salinity. The simulated layer thickness increases from ~20 m in winter to ~60 m in summer. However, the model overestimates the salinity in the top 60 m in spring and underestimates the salinity in the bottom layer in summer. This model deficiency, as mentioned above, may be due to the lack of

precipitation and evaporation processes at the sea surface in the model. In addition, the warm and salty Slope Water intrusion at the shelf break may not be well represented in the model.

3.3 The Nova Scotia Current

We next assess the model performance in simulating the Nova Scotia Current (NSC) using in situ current observations. Figure 12 presents the depth-integrated monthly-mean current produced by submodel L3 of DalCoast-CSS in February 2012, when the NSC transport is at its annual peak (Loder, Hannah, Petrie *et al.*, 2003). The main circulation feature as shown in Figure 12 is that the simulated NSC flows southwestward following the 150 m isobath along the coast. There are two small branches that separate from the main branch of the NSC and flow southward in the offshore direction over the western edge of Emerald and LaHave Basins. The model also produces a westward shelf break jet over the area to the south of the Emerald Bank. The flow pattern described above is consistent with the density-driven currents calculated from historical hydrographic profiles (Sheng and Thompson, 1996) and seasonal circulation in winter

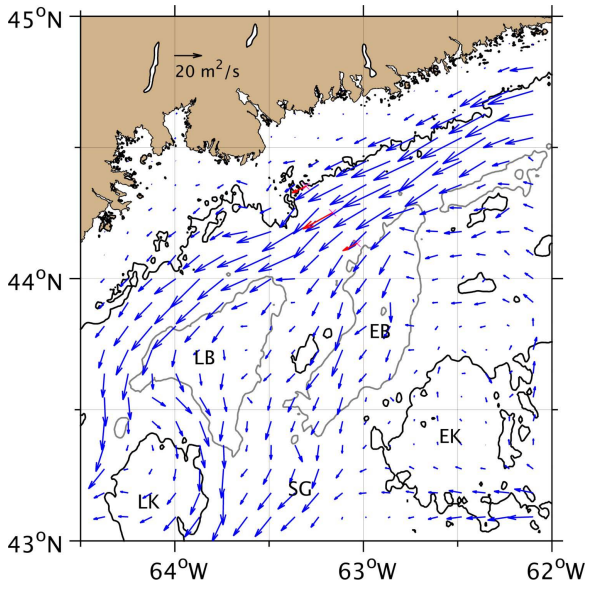

Figure 12. Horizontal distributions of monthly-mean vertically integrated currents in February 2012 in the central SS produced by submodel L3. For clarity, current vectors are plotted at every fifth model grid point. Red arrows represent the observed vertically integrated current. The 100 m and 200 m isobaths are shown in black and gray contours, respectively. The magenta "×" indicates positions of three current moorings. Abbreviations are used for the LaHave Basin (LB), Emerald Basin (EB), LaHave Bank (LK) and Emerald Bank (EK).

diagnosed numerically from the seasonal-mean climatologies of temperature and salinity (Hannah, Shore, Loder *et al.*, 2001).

The NSC has been observed since 2008 using bottom-mounted ADCPs deployed by the Ocean Tracking Network (OTN) (http://oceantrackingnetwork.org) at three locations along a transect from the outside of Halifax Harbour (100 m isobath) to the edge of Emerald Basin (200 m isobath) (upward-pointing solid triangles in Figure 2C). A visual comparison between the monthly-mean current observations (red arrows in Figure 12) and monthly-mean model results suggests that the model is able to capture the magnitude and direction of the NSC in February 2012.

We next assess the model performance in simulating temporal variability of the NSC transport. For simplicity, the NSC transport is defined as the alongshore transport passing through the transect occupied by the three ADCP stations and the positive direction of the alongshore transport is toward northeast (58°T, degrees from true north in a clockwise direction). Figure 13 presents the NSC transport in 2011 and 2012 calculated from currents observed by ADCPs and simulated by submodel L3 of DalCoast-CSS at three locations. The observed time-mean (2008–2014) NSC transport is about −0.4 Sv (Sv ≡ 10^6 m^3 s^{-1}) to the southwest. Seasonal variation in the transport is evident in the observed monthly-mean climatology (2008–2014, the black line with open circles in Figure 13A), with relatively stronger transport in winter and weaker in summer. The observed daily NSC transport has significant synoptic variability. It should be noted that the observed transport in summer 2011 (2012) is stronger (weaker) than the climatology. The simulated NSC transport demonstrates a similar seasonal cycle in comparison with the observed transport. However, the model overestimates the transport in summer 2012. We speculate that the weakening of the observed NSC in summer 2012 is related to the intrusion of abnormally warm Slope Water (Hebert, Pettipas, Brickman *et al.*, 2013). As mentioned earlier, the model has deficiencies in simulating the circulation and associated variability over the Slope Water region. The seasonal transport anomaly (Figure 13B) is then calculated by subtracting the seasonal cycle from the total transport. The observed transport anomaly fluctuates between −0.4 and +0.4 Sv in fall and winter, and the observed amplitudes of the fluctuations are damped in spring and summer. The transport anomalies, including the

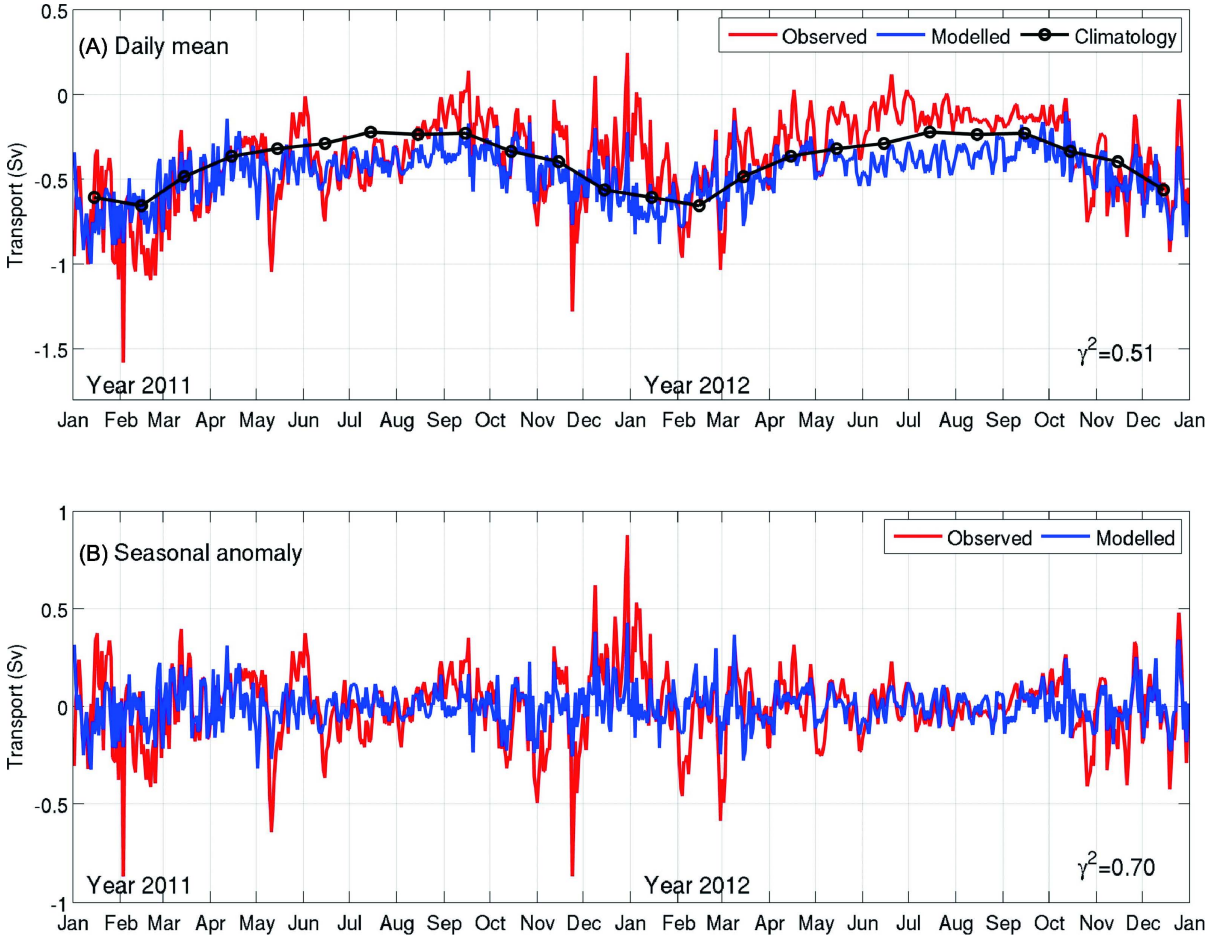

Figure 13. Time series of observed and simulated Nova Scotia Current transport in 2011 and 2012: (A) daily-mean values and (B) seasonal anomalies (calculated by subtracting the seasonal cycle). The simulated results are produced by submodel L3. The black curve in (A) is the monthly-mean transport calculated from the current observations from 2008 to 2014. The Nova Scotia Current transport is calculated using the observed and simulated currents at stations T1, T2 and T3 (Figure 2). Positive values indicate northeastward transport.

seasonality in the fluctuations, are captured reasonably well by submodel L3 with γ^2 = 0.7 in this two-year period. It should be noted that the model underestimates the transport anomaly during strong storm events in winter most likely due to the under-representation of the storm intensity by the regional reanalysis atmospheric forcing used in the model.

4. Physics Controlling Surface Temperature Variability in Summer

DalCoast-CSS is used to identify the main physics controlling the formation of cold surface coastal waters around Nova Scotia in summer as shown in Figure 1. As suggested by previous studies, cold coastal waters are affected by various forcing mechanisms including tidal mixing (Garrett, Keeley and Greenberg *et al.*, 1978; Loder and Greenberg, 1986) and wind-driven coastal upwelling (Petrie, Topliss and Wright, 1987). Three numerical experiments using different configurations of the submodel L2 are conducted as described below:

1. CONTROL RUN (*CR*): The DalCoast-CSS in this experiment is driven by the suite of forcing functions discussed in section 2, including tides, river discharges, atmospheric forcing and open boundary forcing to hindcast the ocean conditions.

2. NO WIND RUN (*NW*): Same as *CR*, except that the local wind stress is set to zero in submodel L2.

3. NO TIDE RUN (*NT*): Same as *CR*, except that the tides are turned off in this experiment. Specifically, tidal elevations (η_t) and tidal currents (u_t) are set to zero along the open boundaries of submodel L2 (see Equation 1).

In experiments *NW* and *NT*, submodel L2 is initia-

lized from the 3D circulation and hydrography on August 1, 2012 produced by the model in *CR* and integrated for one month. The model results of SST and SSS on September 1, 2012 from the above three experiments (Figure 14) are examined to determine the main processes affecting the formation of cold surface waters along the Nova Scotia coast.

The simulated SST in *CR* on September 1, 2012 has significant spatial variations in the study region (Figure 14A-1). The simulated SST at less than ~12°C occurrs mainly over three coastal areas: the BoF and adjacent waters, off Cape Sable, and along the southeastern shore of Nova Scotia. The simulated SST is relatively cold and about 16°C on the eastern SS. The simulated SST is relatively warm and about 20°C on the edge of central and western SS and adjacent Slope Water region. The simulated SST is also relatively warm and about 22°C in the Northumberland Strait ("2" in Figure 14A-1) where the water depth is relatively shallow. In comparison with the observed SST on September 1, 2012 (Figure 1), the simulated SST in *CR* (Figure 14A-1) has similar spatial variations as the observed. The observed cold coastal waters in the BoF and adjacent waters, off Cape Sable and along the southeastern shore of Nova Scotia are reproduced reasonably well by the model.

The simulated SSS in *CR* also has significant spatial variations (Figure 14A-2). The simulated SSS around Prince Edward Island is less than 30.5 psu. The simulated SSS over the coastal waters of the eastern SS is relatively high and up to 31 psu. Two bands of low SSS can be seen on the SS. One band is along the inner shelf with the lowest SSS along the 100 m isobath. The width of this band increases significantly over the western SS. The other band is along the shelf break and only extended to about 64°W. Between the two low SSS bands, there is a pool of relatively high SSS (>32 psu) waters trapped in the middle- and outer- central SS. Beyond the SS, the simulated SSS is relatively high and greater than 32 psu in the Slope Water region. The simulated SSS in the southwest coast of Nova Scotia is also relatively high and greater than 32 psu. Low-salinity waters from the SJR can be seen in the vicinity of the River mouth (red dot in Figure 14A-2). In the middle of BoF, a pool of relatively high SSS (≈31.7 psu) waters is located off Cape Chignecto ("3" in Figure 14A-2).

The simulated SST in the case of *NW* (Figure 14B-1), in which the wind forcing is excluded, showed several distinct features in comparison with the SST in the case of *CR*. The SST in *NW* is relatively uniform and warm (> 26°C) on the SS and adjacent Slope Water region. The cold water band along the southeastern shore of Nova Scotia does not appear in *NW*, which confirms that the formation of this cold water band near the coast is due mostly to the wind forcing. Specifically, the upwelling-favorable wind (Figure 14A-1) pushes the surface water offshore and the cold deep water wells up to the surface near the coast. The SST in the case of *NW* on the SS and in the Slope Water region is warmer than the SST in the case of *CR*, due mainly to the zero simulated latent heat loss from the ocean under the no wind condition. It should also be noted that wind-induced vertical mixing also plays a role in affecting the SST. The cold surface water off Cape Sable is reduced in *NW* in comparison with the results in *CR*, which suggests that latent heat flux and wind-induced vertical mixing enhance the surface cooling in summer in this region. In the BoF, the SSTs in the cases of *NW* and *CR* are highly similar, indicating that physical processes other than wind forcing play an important role in affecting the SST in this region. The SSS in *NW* (Figure 14B-2) also has several distinct features in comparison with the SSS in *CR*. The low SSS band is narrower than the one in *CR* and tightly trapped along the south shore of Nova Scotia with the lowest SSS near the coast. The displacement of the lowest SSS from the coast in *NW* to the ~100 m isobath in *CR* can also be explained by the fact that the upwelling-favorable wind pushes the surface low SSS water offshore and the salty deep water wells up to the surface along the coast. The SSS in *NW* over the Slope Water is higher than the SSS in *CR*. The simulated SSS in the southwest coast of Nova Scotia is reduced significantly in comparison with the results in *CR*. Without the wind forcing (*NW*), the freshwater plume of the SJR is more clearly defined and the BoF is covered by a larger pool of higher SSS waters in comparison with the results in *CR*.

The SST in the case of *NT* (Figure 14C-1), in which the tides are turned off in the model, differs from the SST in the case of *CR* over several coastal areas. The relatively cold waters in the BoF and off Cape Sable do not appear in *NT*. This confirms that tidal mixing plays a very important role in sustaining the well-mixed water over these regions even in summer when the heat flux from the atmosphere is high (Garrett, Topliss and Wright, 1978; Loder and Greenberg, 1986). In addition to tidal mixing, topographic upwelling due to the interaction between tides and bottom

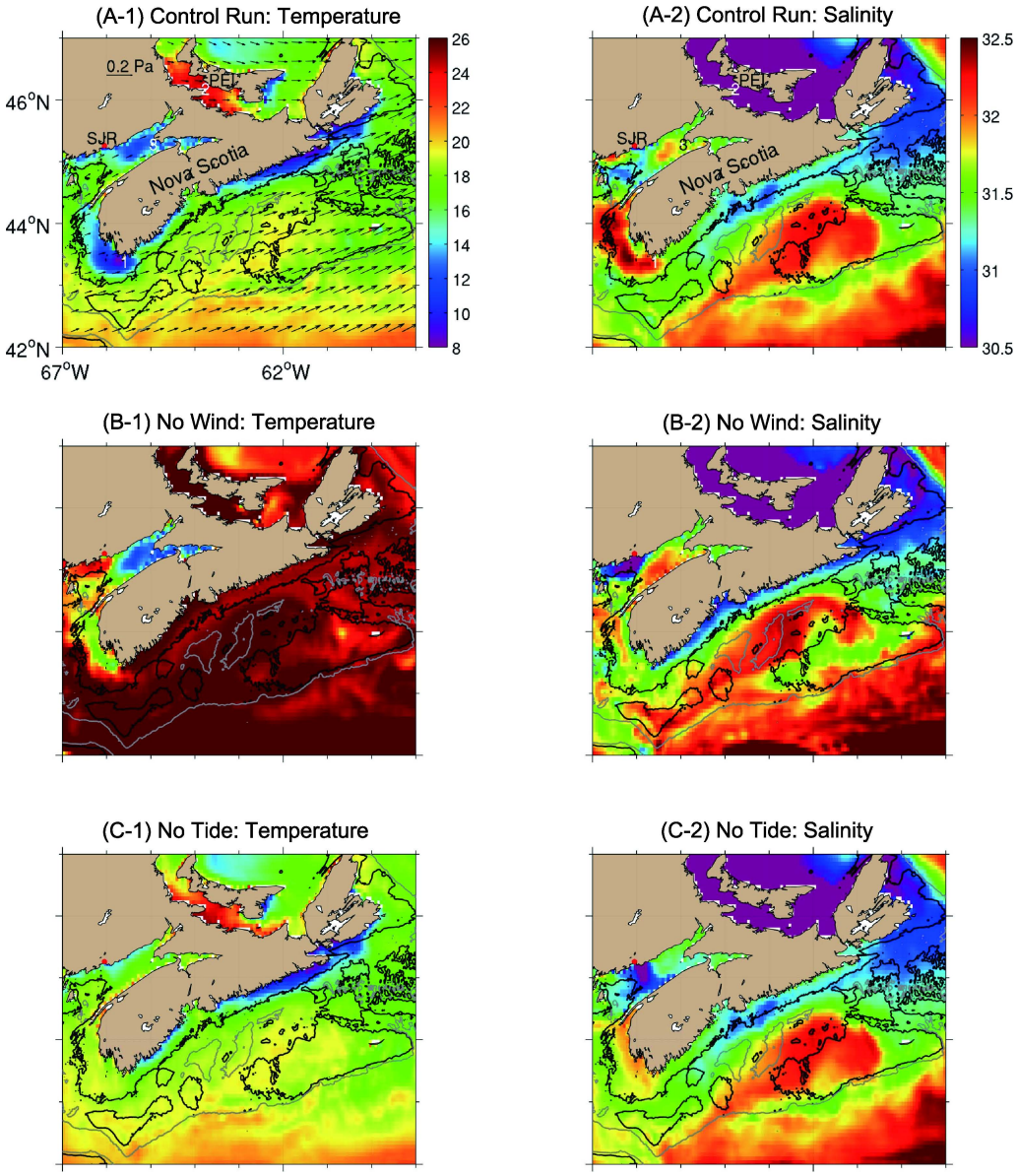

Figure 14. Distributions of sea surface temperature (left) and sea surface salinity (right) in September 1, 2012 in numerical experiments of (A) control run (*CR*), (B) no wind (*NW*) and (C) no tide (*NT*). The time-averaged wind stress used in the model over the previous 48-hours is plotted in (A-1, black arrows). In (A-1) and (A-2), abbreviation is used for Prince Edward Island (PEI) and "1" represents Cape Sable, "2" indicates Northumberland Strait and "3" marks Cape Chignecto. The red dot indicates the mouth of Saint John River (SJR). The 100 m and 200 m isobaths are shown in black and gray contours, respectively.

topography also contributes to the formation of cold surface water off Cape Sable (Tee, Smith and Lefaivre, 1993). On the SS and in the Slope Water region, both the SST and SSS in the case of *NT* are similar to the SST and SSS in the case of *CR*, which indicates that tides play a minor role in affecting the SST and SSS over these regions. The simulated SSS along the southwest coast of Nova Scotia in the case of *NT* is lower than the SSS in the case of *CR*, indicating that tidal mixing also brings high salinity subsurface waters to the surface in this region. Without tides (*NT*), the freshwater plume of the SJR is also well defined. In addition, the pool of high SSS waters off Cape Chignecto is not evident in *NT*, indicating that tides play an important role in the formation of high SSS water in the BoF.

5. Summary

A multi-nested shelf circulation model (DalCoast-CSS) was developed for simulating the variability of circula-

tion and hydrography over the coastal and shelf waters of Nova Scotia. The nested-grid model consists of four submodels downscaling from the eastern Canadian Shelf to the central Scotian Shelf. The nested-grid model was driven by tides, river discharges, and atmospheric forcing. The model performance was assessed by using satellite remote sensing data and in situ observations. The simulated tidal and non-tidal sea levels had good agreement with tide gauge observations; the simulated monthly-mean sea surface temperature and salinity had fair agreement with satellite remote sensing observations; and the simulated daily-mean sea surface temperature outside Halifax Harbour reproduced the observed daily to seasonal variations. The nested-grid model was also able to capture the synoptic variability of the Nova Scotia Current (NSC) transport. However, the model had some deficiencies in simulating the thermocline intensity in summer, the intrusion of warm and salty Slope Water, and the seasonal cycle of the NSC.

The satellite-observed sea surface temperature data revealed that the Atlantic side of Nova Scotia is occasionally surrounded by cold surface waters in summer. The physical processes contributing to the formation of those cold water regions were investigated based on model results in three numerical experiments using DalCoast-CSS. The model results indicated that cold water along the south shore of Nova Scotia is a result of wind-driven coastal upwelling. The formation of cold water in the Bay of Fundy and off Cape Sable is mainly due to tidal mixing and topographical upwelling.

The nested-grid modelling system presented in this study has many applications for future studies concerning the physical environmental conditions over Nova Scotia's coastal and shelf waters. First, DalCoast-CSS will provide better open boundary conditions of the operational circulation forecast system for Halifax Harbour supported by MEOPAR (http://meopar.ca) as a part of an integrated ocean observation and prediction system. Second, DalCoast-CSS will also provide detailed physical oceanic environmental conditions for the studies of marine animal migrations on the Scotian Shelf supported by the Ocean Tracking Network (http://oceantrackingnetwork.org). Finally, assimilating the observations into DalCoast-CSS is planned to further improve the model performance.

Conflict of Interest

No conflict of interest was reported by all authors.

Acknowledgements and Funding

This research was supported by the Marine Environmental Observation Prediction and Response Network (MEOPAR), the Ocean Tracking Network Canada (OTN), the Natural Sciences and Engineering Research Council of Canada (NSERC), and the Lloyd's Register Foundation (LRF). The LRF invests in science, engineering and technology for public benefit, worldwide. S. Shan was also supported by the Killam Predoctoral Fellowship. The authors thank Chris Jones and Emmanuel Devred for their help in obtaining the satellite observations. The authors also thank two anonymous reviewers for their constructive suggestions.

References

Bobanovic J. (1997). Barotropic circulation variability on Canadian Atlantic Shelves. *PhD dissertation, Dalhousie University*.

Dupont F, Hannah C G, Greenberg D A, *et al*. (2002). Modelling system for tides for the Northwest Atlantic coastal ocean. *Canadian Technical Report of Hydrography and Ocean Sciences*, 221: vii + 72p.

Durski S M, Glenn S M and Haidvogel D B. (2004). Vertical mixing schemes in the coastal ocean: Comparison of the level 2.5 Mellor-Yamada scheme with an enhanced version of the K profile parameterization, *Journal of Geophysical Research*, 109(C1): C01015. http://dx.doi.org/10.1029/2002JC001702.

Egbert G D and Erofeeva S Y. (2002). Efficient inverse modeling of barotropic ocean tides, *Journal of Atmospheric and Oceanic Technology*, 19(2): 183–204. http://dx.doi.org/10.1175/1520-0426(2002)019<0183:EIMOBO>2.0.CO;2.

Flather R A and Davies A M. (1976). Note on a preliminary scheme for storm surge prediction using numerical models, *Quarterly Journal of the Royal Meteorological Society*, 102(431): 123–132. http://dx.doi.org/10.1002/qj.49710243110.

Garrett C. (1972). Tidal resonance in the Bay of Fundy and Gulf of Maine, *Nature* 238: 441–443. http://dx.doi.org/ 10.1038/238441a0.

Garrett C, Keeley J and Greenberg D. (1978). Tidal mixing versus thermal stratification in the Bay of Fundy and Gulf of Maine, *Atmosphere-Ocean*, 16(4):403–423. http://dx.doi.org/10.1080/07055900.1978.9649046.

Geshelin Y, Sheng J and Greatbatch R J. (1999). Monthly mean climatologies of temperature and salinity in the western North Atlantic. *Canadian Data Report of Hydrography and Ocean Sciences*, 153: vi + 62p.

Han G and Loder J W. (2003). Three-dimensional seasonal-

mean circulation and hydrography on the eastern Scotian Shelf, *Journal of Geophysical Research: Oceans,* 108(C5): 3136. http://dx.doi.org/10.1029/2002JC001463.

Hannah C G, Shore J A, Loder J W, *et al*. (2001). Seasonal circulation on the western and central Scotian Shelf, *Journal of Physical Oceanography,* 31(2): 591–615. http://dx.doi.org/10.1175/1520-0485(2001)031<0591:SCOTWA>2.0.CO;2.

Hebert D, Pettipas R, Brickman D, *et al*. (2013). Meteorological, sea ice and physical oceanographic conditions on the Scotian Shelf and in the Gulf of Maine during 2012. *Canadian Science Advisory Secretariat Research Document,* 058: v + 46p.

Large W G and Pond S. (1981). Open ocean momentum flux measurements in moderate to strong winds, *Journal of Physical Oceanography,* 11(3): 324–336. http://dx.doi.org/10.1175/1520-0485(1981)011<0324:OOMFMI>2.0.CO;2.

Loder J W and Greenberg D A. (1986). Predicted positions of tidal fronts in the Gulf of Maine region, *Continental Shelf Research,* 6(3): 397–414. http://dx.doi.org/10.1016/0278-4343(86)90080-4.

Loder J W, Hannah C G, Petrie B D, *et al.* (2003). Hydrographic and transport variability on the Halifax section, *Journal of Geophysical Research,* 108(C11): 8003 http://dx.doi.org/10.1029/2001JC001267.

Loder J W, Petrie B and Gawarkiewicz G. (1998). The coastal ocean off northeastern North America: A large-scale view, in A. R. Robinson and K. H. Brink (eds), *The Sea,* 11: 105–133.

Mellor G L. (2004). *Users guide for a three-dimensional, primitive equation, numerical ocean model,* Atmospheric and Oceanic Sciences Program, Princeton University.

Mellor G L and Yamada T. (1982). Development of a turbulence closure model for geophysical fluid problems, *Reviews of Geophysics and Space Physics,* 20(4): 851–875. http://dx.doi.org/10.1029/RG020i004p00851.

Mesinger F, DiMego G, Kalnay E, *et al*. (2006). North american regional reanalysis, *Bulletin of the American Meteorological Society.* 87(3): 343–360. http://dx.doi.org/10.1175/BAMS-87-3-343.

NASA Aquarius project. (2015). Aquarius Official Release Level 3 Sea Surface Salinity Standard Mapped Image Monthly Data V4.0. Ver. 4.0. PO.DAAC, CA, USA. Dataset accessed, viewed 24 July, 2015.

Ohashi K and Sheng J. (2013). Influence of St. Lawrence River discharge on the circulation and hydrography in Canadian Atlantic waters, *Continental Shelf Research,* 58: 32–49. http://dx.doi.org/10.1016/j.csr.2013.03.005.

Ohashi K and Sheng J. (2015). Investigating the effect of oceanographic conditions and swimming behaviours on the movement of particles in the Gulf of St. Lawrence using an individual-based numerical model, *Atmosphere-Ocean,* http://dx.doi.org/10.1080/07055900.2015.1090390.

Orlanski I. (1976). A simple boundary condition for unbounded hyperbolic flows, *Journal of Computational Physics.* 21: 251–269. http://dx.doi.org/10.1016/0021-9991(76)90023-1

Pawlowicz R, Beardsley B and Lentz S. (2002). Classical tidal harmonic analysis including error estimates in MATLAB using T_TIDE, *Computers & Geosciences,* 28(8): 929–937. http://dx.doi.org/10.1016/S0098-3004(02)00013-4.

Petrie B D and Drinkwater K F. (1993). Temperature and salinity variability on the Scotian Shelf and in the Gulf of Maine 1945-1990, *Journal of Geophysical Research,* 98(C11): 20079–20089. http://dx.doi.org/10.1029/93JC02191.

Petrie B D, Topliss B and Wright D G. (1987). Coastal upwelling and eddy development off Nova Scotia, *Journal of Geophysical Research,* 92(C12): 12979–12991. http://dx.doi.org/10.1029/JC092iC12p12979.

Powell M D, Vickery P J and Reinhold T A. (2003). Reduced drag coefficient for high wind speeds in tropical cyclones, *Nature* 422:279–283. http://dx.doi.org/10.1038/nature01481.

Saha S, Moorthi S, Wu X, *et al.* (2011), updated monthly (2016). NCEP Climate Forecast System Version 2 (CFSv2) Selected Hourly Time- Series Products. Research Data Archive at the National Center for Atmospheric Research, Computational and Information Systems Laboratory, Dataset accessed, viewed 4 January, 2016. http://dx.doi.org/10.5065/D6N877VB.

Shan S, Sheng J and Greenan B J W. (2014). Physical processes affecting circulation and hydrography in the Sable Gully of Nova Scotia, *Deep Sea Research Part II: Topical Studies in Oceanography,* 104: 35–50. http://dx.doi.org/10.1016/j.dsr2.2013.06.019.

Shan S, Sheng J, Thompson K R, *et al.* (2011). Simulating the three-dimensional circulation and hydrography of Halifax Harbour using a multi-nested coastal ocean circulation model, *Ocean Dynamics,* 61(7): 951–976. http://dx.doi.org/10.1007/s10236-011-0398-3.

Sheng J, Greatbatch R J and Wright D G. (2001). Improving the utility of ocean circulation models through adjustment of the momentum balance, *Journal of Geophysical Research,* 106(C8): 16711–16728. http://dx.doi.org/10.1029/2000JC000680.

Sheng J and Thompson K R. (1996). A robust method for diagnosing regional shelf circulation from scattered density profiles, *Journal of Geophysical Research,* 101(C11): 25647–25659. http://dx.doi.org/10.1029/96JC01331.

Sheng J, Wright D G, Greatbatch R J, *et al*. (1998). CANDIE: A

new version of the DieCAST ocean circulation model, *Journal of Atmospheric and Oceanic Technology,* 15(6): 1414–1432. http://dx.doi.org/10.1175/1520-0426(1998)015<1414:CANVOT>2.0.CO;2.

Sheng J, Zhai X and Greatbatch R J. (2006). Numerical study of the storm-induced circulation on the Scotian Shelf during Hurricane Juan using a nested-grid ocean model, *Progress in Oceanography,* 70(2-4): 233–254. http://dx.doi.org/10.1016/j.pocean.2005.07.007

Smagorinsky J. (1963). General circulation experiments with the primitive equations, *Monthly Weather Review,* 91(3): 99–164. http://dx.doi.org/10.1175/1520-0493(1963)091<0099:GCEWTP>2.3.CO;2.

Smith P C. (1989). Seasonal and interannual variability of current, temperature and salinity off southwest Nova Scotia, *Canadian Journal of Fisheries and Aquatic Sciences,* 46(S1): s4–s20. http://dx.doi.org/10.1139/f89-275.

Smith P C, Houghton R W, Fairbanks R G, *et al*. (2001). Interannual variability of boundary fluxes and water mass properties in the Gulf of Maine and on Georges Bank: 1993-1997, *Deep Sea Research Part II: Topical Studies in Oceanography,* 48(1-3): 37–70. http://dx.doi.org/10.1016/S0967-0645(00)00081-3.

Sutcliffe Jr. W H, Loucks R H and Drinkwater K F. (1976). Coastal circulation and physical oceanography of the Scotian Shelf and the Gulf of Maine, *Journal of the Fisheries Research Board of Canada,* 33(1): 98–115. http://dx.doi.org/10.1139/f76-012.

Tee K T, Smith P C and Lefaivre D (1993). Topographic upwelling off southwest Nova Scotia, *Journal of Physical Oceanography,* 23(8): 1703–1726. http://dx.doi.org/10.1175/1520-0485(1993)023<1703:TUOSNS>2.0.CO;2.

Therriault J C, Petrie B D, Pepin P, *et al.*(1998). Proposal for a northwest Atlantic zonal monitoring program. *Canadian Technical Report of Hydrography and Ocean Sciences,* 194: vii + 57p.

Thompson K R, Loucks R and Trites R. (1988). Sea surface temperature variability in the shelf-slope region of the northwest atlantic, *Atmosphere-Ocean,* 26(2): 282–299. http://dx.doi.org/10.1080/07055900.1988.9649304.

Thompson K R, Ohashi K, Sheng J, *et al.* (2007). Suppressing bias and drift of coastal circulation models through the assimilation of seasonal climatologies of temperature and salinity, *Continental Shelf Research*, 27: 1303–1316. http://dx.doi.org/10.1016/j.csr.2006.10.011.

Thompson K R and Sheng J. (1997). Subtidal circulation on the Scotian Shelf: Assessing the hindcast skill of a linear, barotropic model, *Journal of Geophysical Research,* 102(C11): 24987–25003. http://dx.doi.org/10.1029/97JC00368.

Urrego-Blanco J and Sheng J. (2012). Interannual variability of the circulation over the eastern Canadian shelf, *Atmosphere-Ocean,* 50(3): 277–300. http://dx.doi.org/10.1080/07055900.2012.680430.

Urrego-Blanco J and Sheng J. (2014). Study on subtidal circulation and variability in the Gulf of St. Lawrence, Scotian Shelf, and Gulf of Maine using a nested-grid shelf circulation model, *Ocean Dynamics* 64(3): 385–412. http://dx.doi.org/10.1007/s10236-013-0688-z.

Wu Y, Tang C L and Hannah C G. (2012). The circulation of eastern Canadian seas, *Progress in Oceanography,* 106: 28–48. http://dx.doi.org/10.1016/j.pocean.2012.06.005.

Yang B and Sheng J. (2008). Process study of coastal circulation over the inner Scotian Shelf using a nested-grid ocean circulation model, with a special emphasis on the storm-induced circulation during tropical storm Alberto in 2006, *Ocean Dynamics* 58(5):375–396. http://dx.doi.org/10.1007/s10236-008-0149-2.